International Journal of Biological Macromolecules 316 (2025) 144567

Contents lists available at ScienceDirect

International Journal of Biological Macromolecules

journal homepage: www.elsevier.com/locate/ijbiomac

Membrane disruption potential of endogenous opioid neuropeptide Dynorphin A and related clinical variants

Eric Catalina-Hernandez [a,b,1], Mario Lopez-Martin [a,b,1], Marcel Aguilella-Arzo [c], Alex Peralvarez-Marin [a,b,*]

[a] Unit of Biophysics, Department of Biochemistry and Molecular Biology, Facultat de Medicina, Av. Can Domènech s/n, Universitat Autònoma de Barcelona, 08193 Cerdanyola del Vallès, Catalonia, Spain
[b] Institute of Neurosciences, Universitat Autònoma de Barcelona, 08193 Cerdanyola del Vallès, Catalonia, Spain
[c] Laboratory of Molecular Biophysics, Department of Physics, University Jaume I, 12071 Castellon, Spain

ARTICLE INFO

Keywords:
Dynorphins
Membrane transport
Neuropeptides
Peptide-bilayer interactions
Membrane disturbing potential
Molecular dynamics simulations

ABSTRACT

Dynorphins are natural neuropeptides that act like opioids but can also cause harmful effects like neurological issues and cell death. Dynorphin A (DynA WT) and its variants (L5S, R6W, and R9C) may disrupt lipid bilayers, leading to pathophysiological effects. Using steered and conventional molecular dynamics simulations, we evaluated how DynA and its variants interact with and penetrate model lipid bilayers. We defined three lipid compositions: neutral, cholesterol-rich and negatively charged, representing different sections of a cell membrane to characterize specific lipid-protein interactions. The R6W peptide cannot find a stable state in any membrane, always returning to the water-bilayer interface. DynA L5S uniquely disturbs neutral lipid bilayers by forming proteolipid pores at the hydrophobic core. DynA WT and L5S are capable to form more stable proteolipid pores in neutral bilayers with cholesterol. L5S and R9C disrupt negatively charged bilayers with cholesterol, again, being able to form stable toroidal pores. The computational strategy presented here allows to study how single amino acid changes in DynA peptides affect their ability to disturb different bilayer compositions.

1. Introduction

Dynorphins are prohormones found in the brain and central nervous system, whose expression is altered in the brain of drug and alcohol abusers and in patients with some neurological disorders [1]. Physiologically, dynorphins are derived from prodynorphin (PDYN) [2] and constitute one of the most basic peptides in the human body [3]. Prodynorphin is cleaved at positively charged residue motifs yielding Big Dynorphin (BigDyn, 32 residues), and can be further processed into Dynorphin A (DynA, 17 residues) and Dynorphin B (DynB, 13 residues) by cleaving the K-R hinge region between them [4,5]. BigDyn and DynA have been previously described to possess internalization into neurons capacity, crossing the cell plasma membrane and leading to ion flow through membranes [6–10], consistent with the formation of membrane pores [11].

DynA interacts with opioid receptors, namely κ-opioid receptor (KOR) and μ-opioid receptor (MOR), and plays a role in pain, stress, and addiction. Besides its opioid effects, DynA has other non-opioid activities, such as anti-amyloidogenic properties [12] or inhibition of *N*-methyl-D-aspartate (NMDA) receptors [13]. Bakalkin et al. identified three different coding mutations within the DynA region in the PDYN gene in a form of the human neurodegenerative disorder spinocerebellar ataxia 23 (SCA23) [14]. The mutations correspond to positions L5, R6, and R9 of DynA, to S (L5S), W (R6W), and C (R9C), respectively. Analysis of DynA wild type (WT) and its clinical variants on striatal neurons concluded that DynA R6W and R9C cause a higher toxicity than DynA WT [14]. In a study -with both neutral and zwitterionic- large unilamellar vesicles (LUVs), DynA R6W and R9C showed the highest degree of leakage, whereas DynA L5S showed the least leakage [15]. Structural studies indicate DynA WT has some N-terminal helical structure upon DMPC binding, while R6W shows helical structure and strong bilayer association, unlike the less structured L5S [16]. In a more recent study, DynA L5S was shown to display increased degradation, whereas DynA R6W and R9C showed increased stability compared to

* Corresponding author at: Unit of Biophysics, Dept. of Biochemistry and Molecular Biology, Facultat de Medicina, Av. Can Domènech s/n, Universitat Autònoma de Barcelona, 08193 Cerdanyola del Vallès, Catalonia, Spain.
E-mail address: alex.peralvarez@uab.cat (A. Peralvarez-Marin).
[1] Equally contributed.

https://doi.org/10.1016/j.ijbiomac.2025.144567
Received 28 November 2024; Received in revised form 15 May 2025; Accepted 21 May 2025
Available online 22 May 2025

DynA WT [17]. Besides, DynA WT and R6W were the most toxic peptides to primary cerebellar neurons. Nonetheless, the membrane disruption mechanism of DynA WT and its clinical variants remains elusive.

Molecular dynamics (MD) simulations have been used to study DynA interaction with membranes. Initially, DynA was found to get inserted with a tilt angle of ~35° with respect to the membrane [18,19]. Then, DynA was found to stay in the outer surface of the membrane when interacting with the κ-opioid receptor [20]. In a more recent study, DynA was found to be able to stabilize pores [21]. However, in order to analyse the membrane disrupting capacity, such as pore formation or membrane translocation, enhanced sampling techniques are needed [22,23].

DynA and the clinical variants show prototypical cell-penetrating peptides (CPP) features [24,25], such as amphiphilicity, positive net charge, α-helix structure propensity upon membrane interaction [26], and actual bilayer translocation in cell lines [6]. Thus, we decided to use a computational method that has been applied to CPP research. Umbrella Sampling (US) [27] has been used in previous studies [23,28], but US is primarily utilized to calculate the barrier of CPP translocation. Coarse-grained MD (CGMD) has also been used to study the translocation of nona-arginine (Arg9) [29], but the information provided by CGMD is limited due to lower resolution [30]. Therefore, we propose the use of adaptive steered molecular dynamics (aSMD), used by Gimenez-Dejoz and Numata [31], and combine it with conventional molecular dynamics (cMD). With this method, we are able to obtain a quantitative result with aSMD, such as the free energy of bilayer crossing, and, since aSMD generates a non-equilibrium state, we are able to characterize the bilayer resistance and the bilayer-peptide interactions with the unbiased cMD simulation, as we used in a previous study to describe the membrane disruption caused by CPPs [32]. Thereafter, we combine aSMD and cMD to characterize the membrane disruption potential of DynA WT and its clinical variants (L5S, R6W, and R9C).

2. Methods

2.1. Systems preparation

The systems were prepared as described previously [32]. Briefly, peptides were modeled in a Colabfold-Alphafold notebook, and relaxed in an explicit solvent system at 310.15 K. AMBER program was used to run the simulations [33]. The AMBER ff14SB [34] force field and periodic boundary conditions were applied, and the SHAKE algorithm [35] was used to restrain the hydrogen atoms, allowing for a 2 fs timestep. 150 mM KCl ions and water TIP3P molecules were used to neutralize and solvate the system. A short minimization (5000 cycles) and NVT equilibration (125 ps) were run with a restraint force of 4.184 $kJ{\cdot}mol^{-1}{\cdot}Å^{-2}$ (1 $kcal{\cdot}mol^{-1}{\cdot}Å^{-2}$) on the peptide, before the unrestrained cMD simulation of 100 ns. Then, clustering analysis was performed to obtain the most representative structure of the peptide, which was further used as initial structure.

Peptide-bilayer systems were built in CHARMM-GUI [36–42] for each relaxed peptide and membrane composition combination. One peptide was added to each system, using the cluster obtained from the peptide relaxation simulation analysis. The peptides were placed at approximately 10 Å from the centre of mass (COM) of the upper leaflet bilayer membrane. The N-terminus or C-terminus of the peptides were not modified at any extent.

Three membrane compositions of 150 lipid molecules -per leaflet- were defined. A neutral bilayer of Dioleoyl phosphatidylcholine (DOPC), namely (1) DOPC (150 lipid molecules), a simple membrane model. A ternary membrane with cholesterol and a different lipid tail was defined: 1,2-Dipalmitoyl phosphatidylcholine (DPPC), DOPC, and cholesterol (CHOL), namely (2) DPPC(50):DOPC(50):CHOL(50). A membrane model containing negatively charged lipids, and to keep a similar proportion as in the previous bilayer, we used: DPPC, DOPC, CHOL, and Dioleoyl phosphatidylserine (DOPS), namely (3) DPPC(38):DOPC(38):DOPS(38):CHOL(38). The same conditions as in the peptide relaxing simulations were used. For the membrane lipids, the Amber Lipid21 [43] force field was selected.

Systems were minimized for 5000 steps and equilibrated during 3.5 ns, starting in the NVT ensemble with positional restraints on the membrane atoms (restraint force of 10.46 $kJ{\cdot}mol^{-1}{\cdot}Å^{-2}$ or 2.5 $kcal{\cdot}mol^{-1}{\cdot}Å^{-2}$), and changing to the NPT ensemble after 500 ps. The system was relaxed for 100 ns of conventional molecular dynamics (cMD). During this step the peptide was kept restrained to avoid peptide-membrane interaction and allow for an unperturbed membrane relaxation (restraint force of 41.84 $kJ{\cdot}mol^{-1}{\cdot}Å^{-2}$ or 10 $kcal{\cdot}mol^{-1}{\cdot}Å^{-2}$). It is important to mention that the lipids are positioned randomly in a symmetric fashion and after such short relaxation, lipid lateral diffusion was not observed. Although our model is a polarity (charge) model and not a lipid phase model, at a given temperature of 310.15 K the bilayers are likely to be in liquid disordered phase, or in a mixed liquid ordered/disordered phase in the case of the complex membranes [44].

2.2. Adaptive steered molecular dynamics (aSMD)

The membrane length (ca. 40 Å) was divided in 8 stages of 5 Å, and 25 replicas were run for each step. The constant force used was 41.84 $kJ{\cdot}mol^{-1}$ or 10 $kcal{\cdot}mol^{-1}$, and a pulling speed of 1 Å/ns (5 ns per step), as discussed in our previous study [32]. After each step, the Jarzynski average [45–47] across all replicas was calculated, and the last frame of the closest replica was used as input for the following step. An aSMD step totalled 125 ns per step and 1000 ns per aSMD simulation, totalling 12 μs for the aSMD part (4 peptides × 3 membrane compositions).

2.3. Conventional molecular dynamics (cMD)

Starting from the last frame of the aSMD, a 100 ns cMD simulation was performed. The same simulating conditions were used as in the previous cases. A total of ~4 μs were run for the final relaxation part, accounting for 100 ns for each of the simulations (100 ns × 4 peptides × 3 membrane compositions x 3 replicas). Besides, 100 ns control simulations have been run for each membrane. We have run all simulations in a workstation with a GPU RTX3080Ti, where it ran at an average velocity of 80 ns per day.

2.4. PMF calculation

The Potential of the Mean Force (PMF) is computed by employing the Jarzynski equality [46], an equation that relates the non-equilibrium work during SMD simulations to the free energy difference between two states, as seen in Eq. (1):

$$G_B = G_A - \frac{1}{\beta}\ln\left\langle e^{-\beta W_{A\to B}}\right\rangle_A \quad (1)$$

where A is the initial state, B the final state, β the Boltzmann constant multiplied by the temperature ($k_B{\cdot}T$), and the tangled brackets indicate the average over multiple trajectories.

Afterwards, the replica with the closest work value to the Jarzynski average is selected as the starting point for the next simulation step. The Jarzynski equality employed in aSMD eliminates trajectories with minimal contributions to the overall PMF, significantly reducing the number of simulations needed for convergence [33].

2.5. Data analysis

Clustering and trajectory analysis was performed using MDAnalysis and PyLipID [48–50]. An in-house Python script was implemented to compute the radius pore size distribution, calculating the minimum pore size in the z axis of the membrane. This script calculates the maximum

distance of the water residues per each membrane z-stack and outputs the minimum radius distance of all the z-stacks per each simulation frame. Matplotlib [51] and Seaborn [52] were used for graphics plotting. UCSF ChimeraX [53,54] and VMD [55] were used for molecular graphics.

2.6. Data availability

Code to reproduce the analysis performed here is available at: https://github.com/APMlab-memb/DynAs_aSMD_cMD.git.

Due to file size limitations, the simulation trajectory file will be shared upon request.

3. Results and discussion

3.1. PMF barrier to membrane crossing

The aSMD process for DynA peptides is represented in Fig. 1. Peptides (Fig. 1A and Table 1) were steered across three types of membranes representing different sections of a cell bilayer (Fig. 1B), which also correspond to energetic barriers to be overcome.

In the process of DynA cell internalization, the peptide first encounters the outer side of the membrane, rich in neutral lipids. Then, it gets inserted into the hydrophobic core of the membrane, where it can find different lipid tails and cholesterol. Finally, DynA internalizes

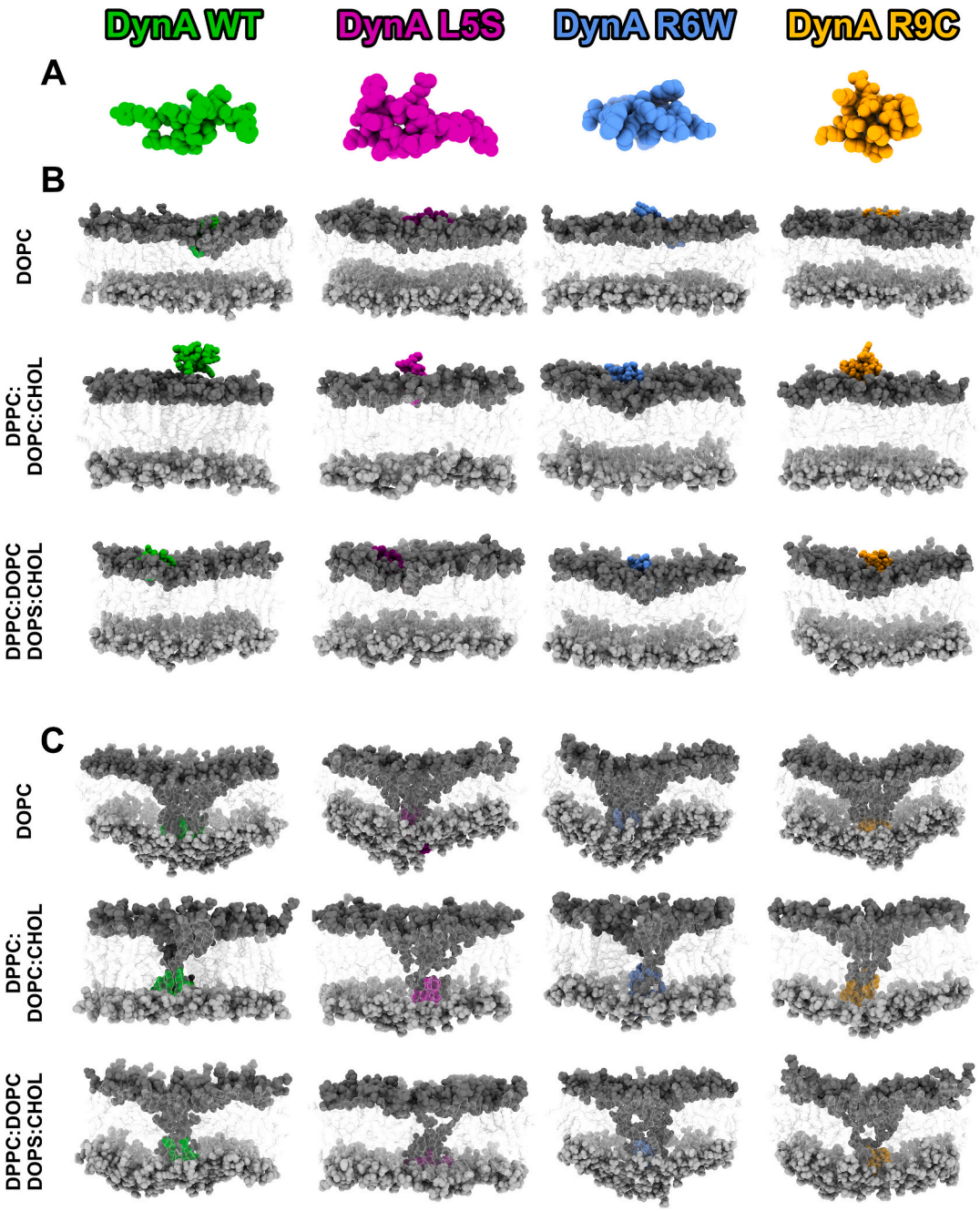

Fig. 1. Initial (A) and final (B) snapshots of the adaptive Steered Molecular Dynamics (aSMD) simulation of DynA WT and its three clinical variants: L5S, R6W, R9C. The timesteps in the three membrane compositions are shown. Peptides are coloured as: DynA WT in light green, L5S in purple, R6W in cornflower blue, and R9C in orange. The polar heads of phospholipids in both the upper and lower bilayers are illustrated in darker and lighter shades of grey, respectively. The lipid tails are portrayed in transparent white. Peptide colours are maintained in the following figures. Waters are omitted for clarity.

Table 1
Characteristics of the peptides used in this study. GRAVY score is calculated from [72].

Peptide	Length	Sequence[a]	Type	Net charge	GRAVY score
DynA WT	17	YGGFLRRIRPKLKWDNQ	Amphipathic	+4	−1.26
DynA L5S	17	YGGF**S**RRIRPKLKWDNQ	Amphipathic	+4	−1.54
DynA R6W	17	YGGFL**W**RIRPKLKWDNQ	Amphipathic	+3	−1.05
DynA R9C	17	YGGFLRRI**C**PKLKWDNQ	Amphipathic	+3	−0.85

[a] Position for mutation in Dyn A WT are underlined, and the residue substitution is indicated in bold in the clinical variants.

through interaction with the inner part of the bilayer, with negatively charged phospholipids. We have tried to model this process with three different membrane compositions: (1) the DOPC bilayer represents the transition from water to the neutral polar head feature of the extracellular/upper leaflet; (2) the DPPC:DOPC:CHOL bilayer represents the transition from the water-bilayer interface to the hydrophobic and rigid bilayer core; and (3) the DPPC:DOPC:DOPS:CHOL as a model for the transition from the hydrophobic core to the negatively charged inner/lower leaflet of the bilayer.

The final step of the aSMD simulation (Fig. 1C) shows the peptide at the lower leaflet of each bilayer in a non-equilibrium state. Moreover, the membrane disturbance exerted is indicated by the polar heads from the upper leaflet dragged down together with the peptide, as a representation of the Defect-Assisted-by-Charge (DAC) phenomenon [56]. To quantify the membrane disruption potential of each peptide upon each bilayer, the PMF barrier was calculated (Fig. 2 and Fig. S1). The peptides have, in average, similar difficulty to traverse the DOPC and DPPC:DOPC:CHOL bilayers (average PMFs of 750 ± 50 and 750 ± 40 kJ·mol^{-1} (or 180 ± 10 and 180 ± 10 kcal·mol^{-1})) compared to DPPC:DOPC:DOPS:CHOL bilayer, with average PMF of 1000 ± 80 kJ·mol^{-1} (240 ± 20 kcal·mol^{-1}).

DynA WT has a high PMF barrier for DOPC, whereas the steering through the DPPC:DOPC:CHOL bilayer is less restrictive, but the DPPC:DOPC:DOPS:CHOL bilayer opposes the strongest PMF barrier to DynA WT crossing (Fig. 2, Fig. S1 and Table 2). These results indicate that DynA WT favors the interaction with different lipid tails and cholesterol. The L5S clinical variant shows higher PMF barriers for DOPC and DPPC:DOPC:CHOL compared to DynA WT, but significantly lower in the DPPC:DOPC:DOPS:CHOL membrane. In fact, in the latter, the PMF barrier for L5S is similar to DPPC:DOPC:CHOL bilayer and lower than the PMF in DOPC. In short, the main barrier for L5S is the partition in the upper leaflet of the bilayer, whereas the insertion to the hydrophobic core and the partitioning in the lower leaflet are energetically more

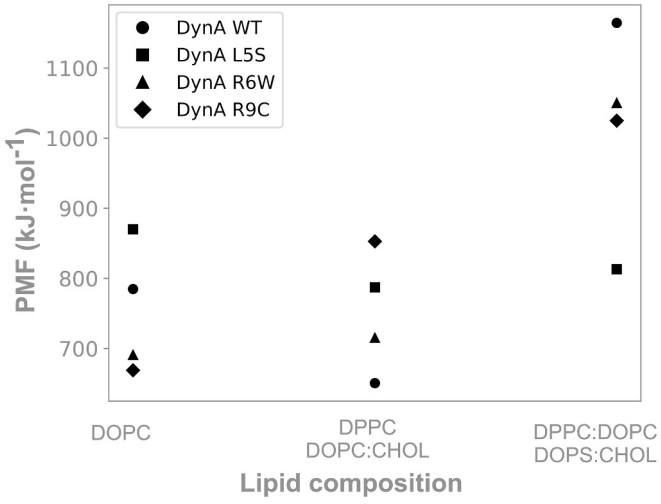

Fig. 2. Potential of Mean Force (PMF) of peptides with respect to the membrane composition. Size and colour indicate energy. The values indicated correspond to the last value (highest energy) of the PMF analysis. PMF profiles and the PMF of all the replicas are shown in Fig. S1.

favourable. The PMF barrier for WT is lower than L5S in the first two membranes and higher in the negatively charged membrane, indicating that the hydrophobic-to-polar substitution allows better stabilization in the lower leaflet, but encounters more difficulties in partitioning in the upper leaflet and inserting in the hydrophobic core. The R6W and R9C clinical variants have a lower PMF barrier in DOPC and DPPC:DOPC:DOPS:CHOL bilayers compared to DynA WT, due to the R substitution affecting water interactions and, thus, facilitates partition in the water-bilayer or bilayer-water interfaces, respectively. In the DPPC:DOPC:CHOL, R6W and R9C show higher PMF barriers, indicating that the R-to-W and R-to-C substitutions hinder the insertion in the membrane's hydrophobic core. Thus, in terms of energy, DynA R6W and R9C show preference for the upper leaflet polar heads-hydrophobic bilayer interface, WT inserts at the hydrophobic core bilayer section, and L5S shows easier partitioning in the lower leaflet polar heads-water interface.

To compare DynA peptides values with previously studied CPPs using the same force field [31,32], we performed simulations of DynA in a DPPC membrane (Table S1). The calculated PMF values were comparable to those previously obtained for CPPs, suggesting that DynA peptides have similar energy requirements for translocation. Moreover, when extending the comparison to other forcefields, a wide range of PMF values is observed. For instance, in a study with DOPC membrane and GROMOS87 force field, the cyclic Arg9 was reported to require approximately 120 kJ·mol^{-1} to reach the bilayer centre in a path where the pore was forced and 200 kJ·mol^{-1} in a pore-free path [28]. In parallel, the TAT peptide required ~300 kJ·mol^{-1} to reach the bilayer centre in a DOPC membrane using the GROMOS96 53a6 force field [57]. Moreover, coarse grained studies(Martini 2.0 force field for Arg and waters and Martini 2.2 polarizable for lipids and ions, in a DPPC membrane) reported similar values for Arg9 and cyclic Arg9, ~330 kJ·mol^{-1} in a pore-free path and ~ 240 kJ·mol^{-1} in a pore-forming path in order to reach the bilayer centre [29]. Thus, these force fields and methods can potentially yield PMF values in the same range as the ones described in this study when considering all the bilayer length. Besides, the OPLS-AA force field yielded a PMF value of ~60 kJ·mol^{-1} for the translocation of a single arginine [58], whereas the CHARMM36 force field resulted in a PMF of ~300 kJ·mol^{-1} for the complete translocation of an Arg9 in a DOPC/DOPG (4:1) membrane with the application of an electric field of 0.05 V/nm [59]. In conclusion, these results indicate that PMF values can be strongly influenced by the choice of force field, thus caution is needed when comparing simulations performed with different force fields [60], and comparisons should be limited to simulations using the same force field.

3.2. Peptide-induced membrane disruption

After the aSMD simulation, which ends in a non-equilibrium situation through the steering process, the molecular distribution is similar for all cases: the peptide has been steered into the lower part of the bilayer and is close to the polar heads of the lipids in the lower part of the bilayer, defining the starting point for the three 100 ns cMD replicas (Fig. 1C). The polar heads in the upper leaflet have been dragged with the peptide in the aSMD, being able to enter in contact with the polar heads in the lower leaflet and creating a continuous flow of water between both compartments, defined as a water pore (of approximately 10 Å, see Figs. S2A and S3). Nonetheless, this water channel is transient and

Table 2
PMF values and simulation results for DynA variants in three lipid membrane compositions.

Peptide	Lipid membrane								
	DOPC			DPPC DOPC:CHOL			DPPC:DOPC DOPS:CHOL		
	PMF (kJ·mol^{-1})	State	Pore size (Å)[a]	PMF (kJ·mol^{-1})	State	Pore size (Å)[a]	PMF (kJ·mol^{-1})	State	Pore Size (Å)[a]
DynA WT	790 ± 10	Return (100 %)	NA	650 ± 10	Pore (100 %)	2.42 ± 0.08	1160 ± 10	RETURN (100 %)	NA
DynA L5S	870 ± 10	Return (66 %) Pore (33 %)	1.38 ± 0.08 (66 %) 5.45 ± 0.8 (33 %)	790 ± 10	Pore (100 %)	1.33 ± 0.07	810 ± 10	Pore (100 %)	4.71 ± 0.08
DynA R6W	690 ± 10	Return (100 %)	NA	720 ± 10	Return (100 %)	NA	1050 ± 10	Return (100 %)	NA
DynA R9C	670 ± 10	Return (100 %)	NA	850 ± 10	Return (100 %)	NA	1020 ± 10	Pore (66 %) Return (33 %)	0.87 ± 0.05 (66 %) NA (33 %)

[a] Average pore radius during the last 80 ns of the cMD simulation; NA, not applicable.

can be stabilized or rapidly closed in the cMD simulation (Figs. 3 and S2B).

The cMD simulation will explore whether the aSMD simulation has reached a close-to-equilibrium state. In Fig. 3 the last step of the 100 ns cMD is shown, while the water distribution is shown in Fig. S2B. All simulations that contain a pore channel, were extended until 500 ns (or until the channel closes) in order to analyse pore stability. DynA WT returns to the upper leaflet in DOPC and DPPC:DOPC:DOPS:CHOL, but WT is able to induce a strong membrane disturbance represented by a stable water-based pore channel (pore stable during the 500 ns

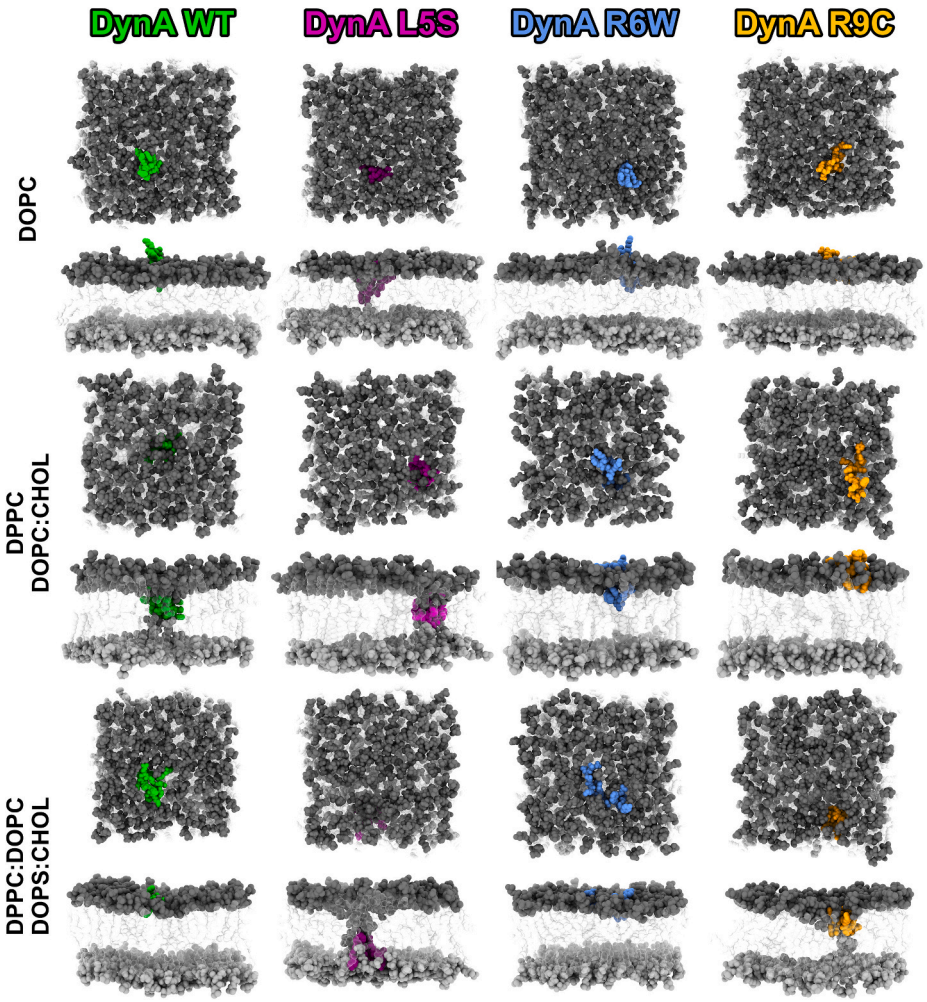

Fig. 3. Illustrative representation of the peptide location in the 3 membrane compositions after the 100 ns of conventional MD (relaxation). Top (top) and side (bottom) poses are shown for each case. The colour code is the following: DynA WT in light green, L5S in purple, R6W in cornflower blue, and R9C in orange. The polar heads of phospholipids in upper and lower bilayers are illustrated in darker and lighter shades of grey, respectively, while the lipid tails are portrayed in transparent white. Waters are omitted for clarity.

simulations) in DPPC:DOPC:CHOL (Table 2, Figs. S2B and S3). DynA L5S shows a stronger membrane disturbing behaviour compared to WT, as L5S induces a transient pore (duration of ca. 80 ns) in two out of the three replicas in DOPC, and a more stable pore channel (ca. 220 ns) in the third DOPC replica and in DPPC:DOPC:CHOL and DPPC:DOPC:DOPS:CHOL bilayers (stable over 500 ns) (Table 2, Figs. S2B and S3). DynA R6W returns to the upper leaflet in all membrane compositions (Table 2). Last, DynA R9C returns to the upper leaflet in the first two membrane compositions but is able to form a pore in DPPC:DOPC:DOPS:CHOL (in two out of the three replicas of ca. 160 ns approximately), arguing for an easier interaction with the lower leaflet owing to the negative charge in the polar heads (Table 2). Overall, we observe two different results: return to the upper leaflet, and pore formation. In the first case, the peptide breaks the new interactions with the polar heads in the lower leaflet, again dragging the polar heads back to the upper leaflet. In the pore formation, the interaction between the polar heads of both leaflets opens a channel that allows water flow between the two water compartments.

In Fig. 4, we show electron density of all the systems to observe the pore formation induced by peptide-bilayer interaction. We see how there is a higher density of water and polar heads in the middle of the bilayer for DynA L5S in DOPC, DynA WT and L5S in DPPC:DOPC:CHOL, and DynA L5S and R9C in DPPC:DOPC:DOPS:CHOL, demonstrating the pore formation. The importance of polar heads and peptides (Figs. 3 and 4) in the pore formation leads to discuss that the kind of pores observed in this study are toroidal pores, where the peptide and polar heads in both leaflets interact, allowing water molecules to cross. Besides, peptides seem to have an important role in pore formation and stabilization, as seen in other studies [61,62].

Pore formation requires that the peptide drags lipid polar heads from the upper leaflet along during the aSMD process. These polar heads remain hydrated by surrounding water molecules which protect them from the hydrophobic membrane environment. Peptide drags lipids from the upper leaflet lipids and contacts the polar heads in the lower leaflet, leading to the interaction of waters from both compartments, ultimately opening a water channel [63]. These toroidal pores, as discussed before, are characterized by the presence of the peptide, lipid polar heads, and water, as illustrated in Figs. 3, 4, and S2.

3.3. Specific peptide-lipid interactions

To discuss the effect of lipid composition in the peptide-lipid interactions, lipid order parameter, membrane thickness, and area per lipid have been analysed (Fig. S3). Lipid order parameter analysis measures the orientation of the lipid chains with respect to the bilayer normal [64]. Our results show that membranes are well organized, and no significant differences are observed between membranes regardless of the type of peptide-bilayer interaction or no peptide (control membranes). In parallel, membrane thickness and area per lipid results are related. DOPC membranes show the smallest membrane thickness (approximately 37 Å) and area per lipid (approximately 68 $Å^2$), indicating that DOPC is the most compact membrane. In DPPC:DOPC:CHOL membranes, the addition of a different lipid tail (DPPC) reduces the membrane compactness, increasing membrane thickness (~42 Å) and area per lipid (~76 $Å^2$). In previous studies, the addition of cholesterol was linked to a decrease in area per lipid [65], but this effect seems to be counterbalanced by the addition of different lipid tails. Lastly, DPPC:DOPC:DOPS:CHOL membranes showcase a decrease in membrane thickness (~40 Å) and area per lipid (~67 $Å^2$), caused by the addition of negatively charged lipids (DOPS), which tighten the membrane [66].

Membrane behaviour can also be related to the fluctuations in PMF values, indicative of the resistance offered by the bilayer to the peptide crossing. DOPC and DPPC:DOPC:CHOL showcase, on average, similar PMF values. Looking at membrane thickness and area per lipid, DPPC:DOPC:CHOL should have a lower PMF value since the membrane is less packed, leading to an easier penetration [67]. Cholesterol triggers a reduced efficiency in CPP translocation [68] and is able to counterbalance the effect of different lipid tails. In DPPC:DOPC:DOPS:CHOL, the membrane is more densely packed than DPPC:DOPC:CHOL (lower membrane thickness and area per lipid), and negative lipids increase peptide adsorption in the upper leaflet [66], ultimately requiring higher energy to break these interactions when internalising. Overall, these

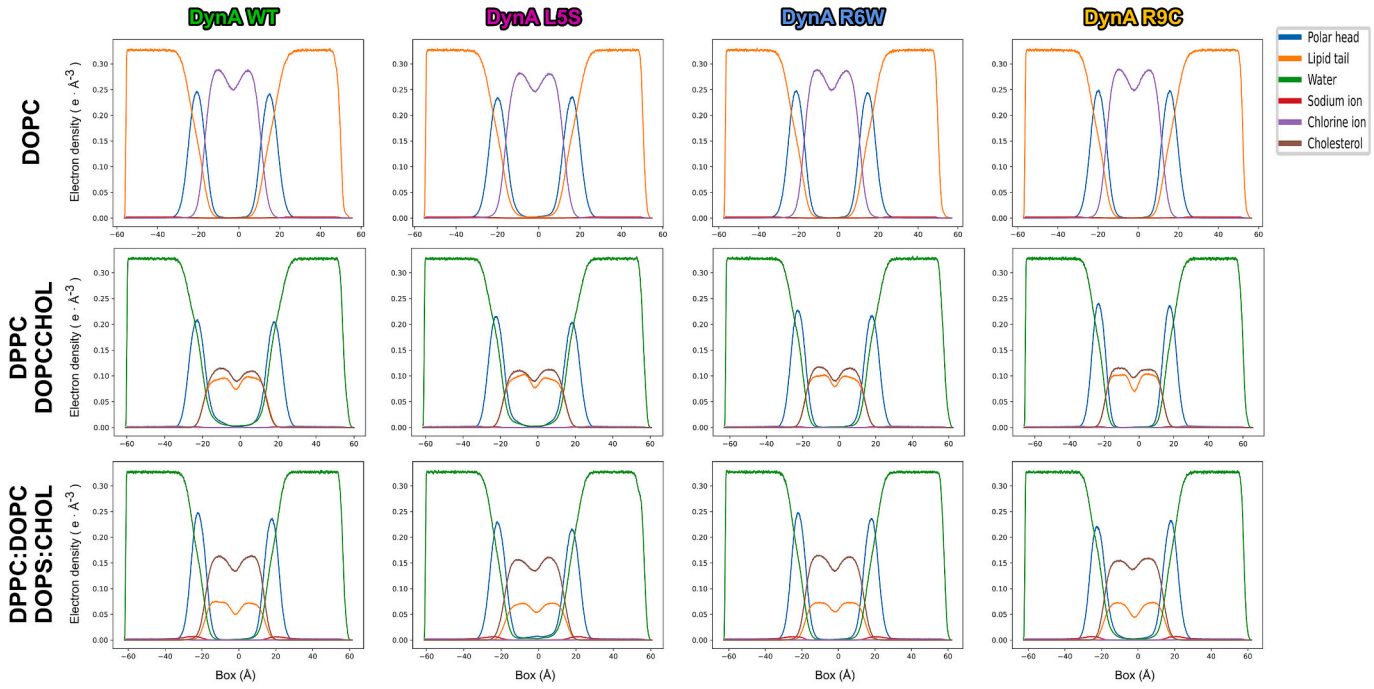

Fig. 4. Electron density plots of DynA WT and its clinical variants in the three membrane compositions. Blue refers to the polar heads, orange to lipid tails, green to waters, red to sodium ion, light blue to chlorine ion and marron to cholesterol (only in second and third membranes). The most representative replica is shown for all simulations.

details cause the highest increase in PMF value of the study.

Analysis of peptide residue occupancy and the interactions with polar heads of the phospholipids in the upper and lower leaflets is shown in Fig. 5. Occupancy, analysed with PyLipID [50], is defined as the percentage of simulation time during which the peptide residue is in contact with the polar head of the phospholipids. Thus, the values shown in Fig. 5 represent the average occupancy during the cMD simulation. DynA WT has five positively charged residues: R6, R7, R9, K11, and K13. In DOPC, R6, R7, and R9 interact with the polar heads, in DPPC:DOPC:CHOL these are R6, R7, K11, and K13, and in DPPC:DOPC:DOPS:CHOL, R7, R9, and K13 are key in the interaction with the polar heads. K/R neighbouring residues also show high occupancy. There is a high interaction zone in residue Y1 (extended to G2 in DOPC, to G3 in DPPC:DOPC:CHOL, and to F4 in DPPC:DOPC:DOPS:CHOL), which has been shown in NMR experiments by Lind et al. [69]. The only DynA residue with negative charge (D15) shows lower occupancy compared to surrounding residues.

The replacement of a hydrophobic residue by a polar residue in L5S facilitates interaction with the PC polar heads (S5 has higher occupancy than L5 in all cases) and the peptide global interactions with the polar heads in DOPC and DPPC:DOPC:DOPS:CHOL membranes. In the cases of DynA R6W and R9C, both mutations entail the loss of a positively charged residue (R). In general, interactions are maintained or shifted towards another part of the peptide. Nonetheless, the lack of R9 in R9C is easily spotted in DPPC:DOPC:DOPS:CHOL, since it is the peptide with the least interaction with PS polar heads.

DynA L5S in DOPC, DynA WT and L5S in DPPC:DOPC:CHOL, and DynA L5S and DynA R9C in DPPC:DOPC:DOPS:CHOL interact with both the upper and lower leaflets. This is the key to toroidal pore formation, since the peptide "complexes" with the phospholipids due to the interaction between positively charged residues and the negatively charged phosphate groups of polar heads [70]. Water molecules solvate positively charged residues (K, R) and their neighbours, leading to the connection of water molecules across both spaces and subsequent pore formation.

The presence of cholesterol in the DPPC:DOPC:CHOL bilayer system introduces a new variable that has not been previously proposed in the DynA clinical variants literature [15–17]. To assess the residue relevance in the hydrophobic core of the bilayer, we analyse the peptide residue occupancy at the cholesterol and lipid tails level (Fig. S4). Hydrophobic (L and I), apolar (P and G), and aromatic (F, W and Y) residues mediate the interaction with the lipid tails. For DynA WT, the interaction with cholesterol happens in both leaflets of the DPPC:DOPC:CHOL and DPPC:DOPC:DOPS:CHOL bilayers, mediated by hydrophobic residues such as L5, I8, and L12, aromatic residues such as Y1, F4, and W14, apolar P10, and charged R9 and D15. In the DynA L5S, most cholesterol interactions are gone, shifted towards Y1, I8, R9, K13, and W14. For R6W, the lost R shifts cholesterol interaction towards the F4-I8 hydrophobic/aromatic patch, and W14 in DPPC:DOPC:DOPS:CHOL. The lost R in R9C restricts the cholesterol interaction to Y1, F4, L5, R7, K11, and W14 in the upper leaflet. In general terms, the presence of negatively charged lipids in the DPPC:DOPC:DOPS:CHOL bilayer, dampens the DynA:cholesterol interaction.

3.4. Global bilayer effects

Cell penetrating peptides (CPPs) and antimicrobial peptides (AMPs) disrupt bilayers through specific mechanisms, with dynorphins—neuropeptides with CPP/AMP potential—proposed to induce cytotoxicity via plasma membrane poration [32]. In a previous computational study, we characterized the membrane disruption potential of canonical CPPs [32]. Here we extend that approach to neuropeptides, such as DynA, using symmetric bilayers to model: (1) peptide partitioning at the water-bilayer interface on the extracellular side (DOPC); (2) peptide transition through the hydrophobic core (DPPC:DOPC:CHOL); and (3) interactions with negatively charged lipids on the cytosolic side (DPPC:DOPC:DOPS:CHOL). Results show that DynA L5S induces strong membrane poration, WT and R9C moderate poration, and R6W no poration, by reaching different stages at the bilayer (Fig. 6).

Comparing the peptide penetration (Fig. 6) and the PMF barrier (Fig. 2, Table 2), we observe the following trend: DynA WT faces high

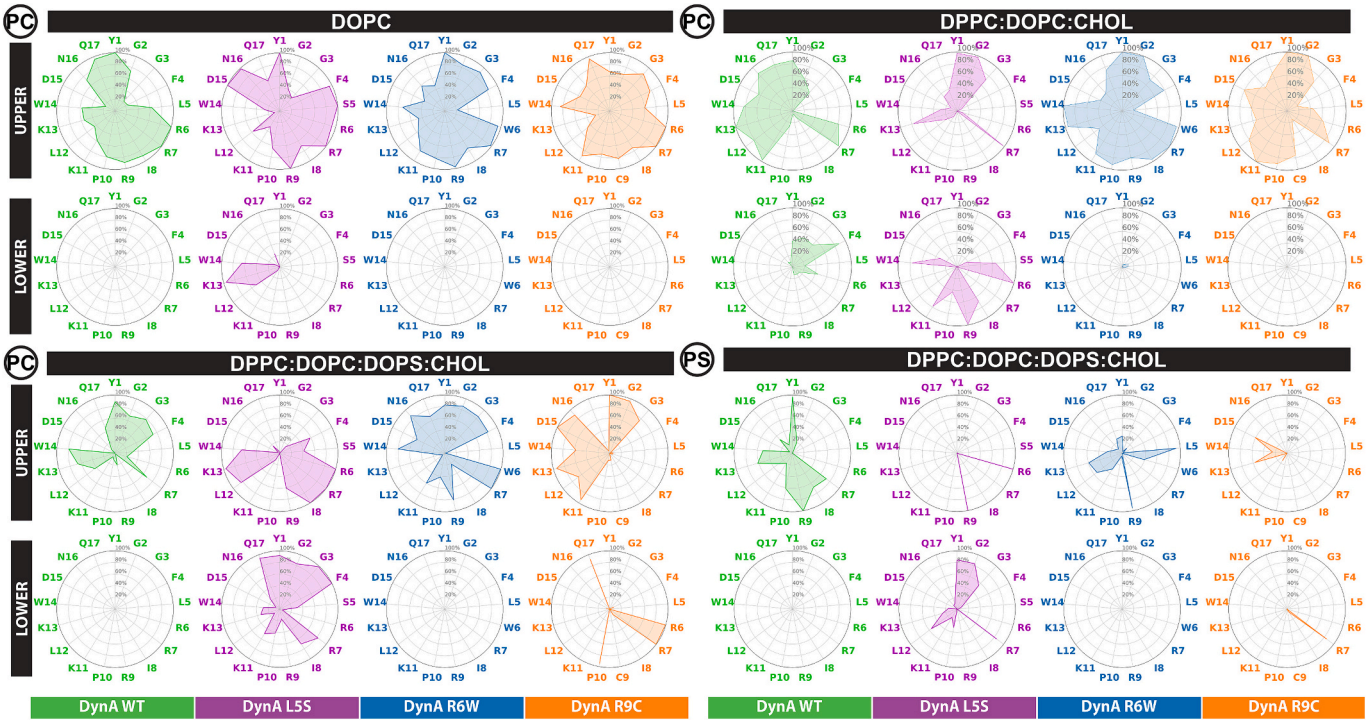

Fig. 5. Occupancy of the DynAs residues by the polar head of the lipid bilayer in upper and lower leaflets. Polar heads pertaining to PC lipids are shown for the three bilayers. PS interaction is also shown for DPPC:DOPC:DOPS:CHOL. The most representative replica analyses are shown for all simulations.

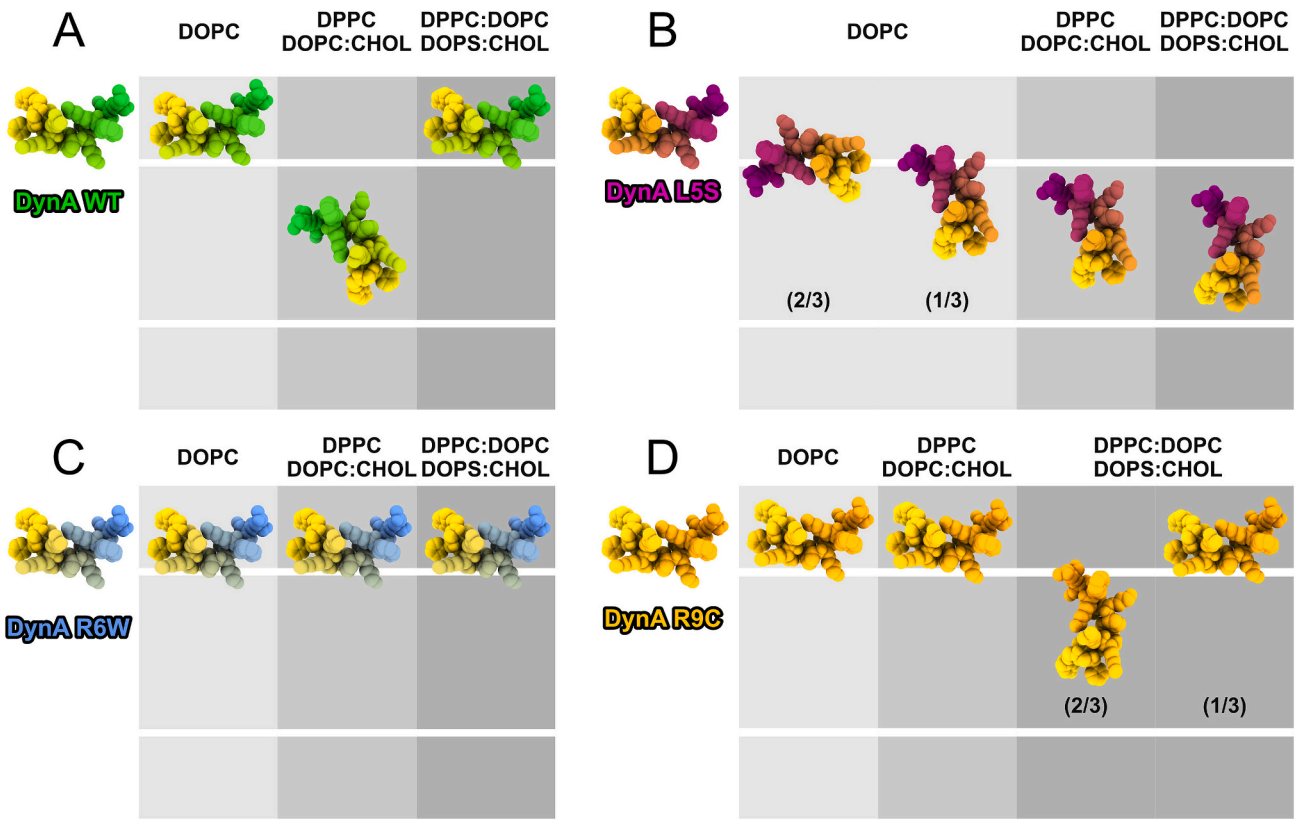

Fig. 6. Final position and orientation of the peptide in the different bilayer compositions. The peptides are coloured from N to C-terminal with a gradient from gold to its respective colour: DynA WT in green, L5S in purple, R6W in cornflower blue, R9C in orange. The bilayer is represented in grey, and darker shades of grey represent higher bilayer complexity: DOPC in light grey, DPPC:DOPC:CHOL in grey, DPPC:DOPC:DOPS:CHOL in dark grey. The white lines differentiate between upper/outer part of the bilayer, hydrophobic core and lower/inner part of the bilayer. The ratios in DynA L5S DOPC and R9C DPPC:DOPC:DOPS:CHOL indicate the ratio of behaviours seen in replicas. If ratios are not shown, 100 % agreement between replicas is observed.

PMF barrier to cross the DOPC membrane (PMF value of 790 kJ·mol^{-1}) and it is not able to get stabilized by forming a pore, contrary to what its observed in DPPC:DOPC:CHOL (PMF value of 650 kJ·mol^{-1}), where the peptide faces a lower PMF requirement and it is able to induce pore formation. In DPPC:DOPC:DOPS:CHOL, DynA WT finds the highest resistance to bilayer crossing (1160 kJ·mol^{-1}), resulting in rapid relocation in the upper leaflet. Overall, DynA WT seems to be able to get stabilized in the hydrophobic core of the membrane, but it encounters difficulty getting adsorbed in the upper leaflet or reaching the lower leaflet. For DynA L5S, the highest resistance to the bilayer crossing is in DOPC (870 kJ·mol^{-1}), which results in more or less stable (pore duration ranges between 80 and 220 ns) pore formation. Then, DynA L5S finds less resistance in the bilayer crossing in DPPC:DOPC:CHOL and DPPC:DOPC:DOPS:CHOL bilayers (780 and 810 kJ·mol^{-1}, respectively) and, thus, L5S is able to porate the bilayer in both cases. In fact, DynA L5S is the only peptide that does not show a considerable increase in the barrier energy when comparing DPPC:DOPC:CHOL to DPPC:DOPC:DOPS:CHOL PMF values. This similarity can be related to the fact that it is the only peptide that is able to form a 500 ns-stable pore in the DPPC:DOPC:DOPS:CHOL bilayer, arguing that it does not encounter high energy barrier to diffuse from the hydrophobic core to the inner leaflet, as opposed to DynA WT. DynA R6W shows a similar barrier to cross the DOPC and DPPC:DOPC:CHOL membranes (640 and 720 kJ·mol^{-1}, respectively), but it is not able to induce poration in any of the cases. In the DPPC:DOPC:DOPS:CHOL bilayer, the PMF increases (1050 kJ·mol^{-1}, respectively) and does not seem to allow the R6W peptide for any membrane disturbance. In short, DynA R6W seems to be able to get adsorbed in the outer leaflet, but without being able to form a pore to access the hydrophobic core. Lastly, for DynA R9C the PMF barrier is low in DOPC, but high in DPPC:DOPC:CHOL and DPPC:DOPC:DOPS:CHOL (670 kJ·mol^{-1}, 850 kJ·mol^{-1}, and 1020 kJ·mol^{-1}, respectively), and only allows for a transient poration (of 160 ns) in DPPC:DOPC:DOPS:CHOL. However, DynA L5S in DOPC (highest PMF value) or DynA WT in DPPC:DOPC:CHOL (lowest PMF value) demonstrate that the PMF is not the sole determinant of membrane disruption, as these peptides show large PMF values, but are still able to induce pore formation. This behaviour indicates that there are more factors affecting the membrane disruption potential, such as peptide-lipid interactions, the disposition of positively charged residues (R, K), peptide orientation or secondary structure. In fact, peptide secondary structure was analysed to check for trends between any secondary structure, PMF fluctuation and/or membrane poration. Nonetheless, no relation was found between these behaviours (Fig. S5), maybe because longer simulation timescales are required to observe meaningful changes in secondary structure, which will be tackled in a further study.

The N-terminus Y1 residue in DynA WT, L5S, and R9C orients towards the hydrophobic core as a prerequisite to poration (Fig. 6), which agrees with experimental studies [69]. DynA peptides form toroidal pores with lipophilic residues facing lipid tails, and hydrophilic residues coordinated with the waters in the inner side of the pore (Fig. S6 and Fig. S7). Specific residues in DynA WT (L5, R6, R9) are crucial for membrane interaction of clinical variants at both polar head and hydrophobic core levels. WT, L5S, and R9C peptides can form water pores stable over 100 ns, agreeing with a pathological mechanism of DynA through plasma membrane poration [11,21], also observed in our simulations. L5S exhibits lower energy barriers and consistent pore formation across all bilayers, like what should be expected from CPPs [32]. In fact, CPPs can decrease the potential of resting cells to low values, in which spontaneous pore formation is possible [71]. Our results may indicate difference to previous liposome leakage experiments, which, as

discussed before, reveal that all DynA variants cause leakage, except L5S in large unilamellar vesicles [15]. Thus, DynA activity may be dependent on membrane compositions [17], whereas Madani et al. used a specific POPC/PG composition, here we use DPPC, DOPC/PS and cholesterol. Overall, DynA peptides, particularly L5S, WT, and R9C, demonstrate stronger water pore-formation potential compared to canonical CPPs. Thus, our method allows for the observation of pore formation and subsequent stabilization or pore closure due to upper or lower leaflet stabilization. DynA WT and the clinical variants show certain peptide aggregation/self-assembly, introducing a peptide concentration factor [17], thus further computational studies considering peptide self-assembly at or in the bilayer [21] should be pursued.

4. Conclusions

In this study, we employed a combination of adaptive steered molecular dynamics (aSMD) and conventional MD (cMD) simulations to investigate the membrane-disrupting potential of DynA WT and its clinical variants. Our results suggest that DynA peptides, particularly DynA L5S, exhibit comparable or lower potential of mean force (PMF) values than canonical CPPs, indicating potential CPP-like behaviour. cMD simulations further support this by showing that DynA L5S consistently induces stable pore formation across diverse membrane compositions, while other variants display distinct, bilayer-dependent behaviours.

We acknowledge that aSMD introduces artificial steering forces to accelerate rare events such as membrane translocation, which in biological systems are driven by a complex interplay of membrane potential, peptide cooperativity, lipid heterogeneity, and thermal fluctuations. While these factors are not explicitly modeled, aSMD enables exploration of translocation pathways within accessible timescales. Importantly, the timescales accessible to molecular dynamics simulations—typically in the range of nanoseconds to microseconds—remain orders of magnitude shorter than those of biological peptide translocation, which can occur over milliseconds to minutes. This discrepancy necessitates the use of enhanced sampling techniques to capture relevant events within computationally feasible timeframes.

The subsequent cMD simulations provide an unbiased view of membrane perturbation, offering complementary insights into the stability and consequences of these events. Although PMF values derived from aSMD are sensitive to the choice of force field and pulling protocol, relative PMF trends across membrane compositions remain informative. Future work should incorporate more biologically realistic membrane models—featuring lipid asymmetry, phase separation, and membrane potential—as well as varied peptide:lipid ratios and initial configurations to better capture physiological complexity.

Despite these limitations, our combined aSMD/cMD approach remains a valuable tool in computational biophysics. It enables mechanistic insights into peptide-membrane interactions that are difficult to access experimentally and complements in vitro and cellular studies by providing atomistic resolution. Our findings support the continued development and application of enhanced sampling techniques to advance our understanding of bioactive peptide function and membrane dynamics.

Supplementary data to this article can be found online at https://doi.org/10.1016/j.ijbiomac.2025.144567.

CRediT authorship contribution statement

Eric Catalina-Hernandez: Writing – review & editing, Writing – original draft, Investigation, Formal analysis, Conceptualization. **Mario Lopez-Martin:** Writing – review & editing, Supervision, Investigation, Conceptualization. **Marcel Aguilella-Arzo:** Writing – review & editing, Resources, Methodology, Funding acquisition. **Alex Peralvarez-Marin:** Writing – review & editing, Writing – original draft, Supervision, Resources, Project administration, Funding acquisition, Conceptualization.

Funding sources

Authors acknowledge financial support by the Spanish Government Grant PID2020-120222GB-I00 (to A.P.-M.) and PID2022-142795NB-I00 (to M.A.-A) funded by MCIN/AEI/10.13039/501100011033, Ministerio de Universidades Margarita Salas Award (MGSD2021-10 to M.L.-M.) and Universitat Autònoma de Barcelona predoctoral fellowship (B21P0033 to E.C.-H.) and Universitat Jaume I project UJI-B2022-42 (to M.A-A).

Declaration of competing interest

The authors declare that they have no known competing financial interests or personal relationships that could have appeared to influence the work reported in this paper.

Data availability

Data will be made available on request.

References

[1] C. Ménard, H. Herzog, C. Schwarzer, R. Quirion, Possible role of dynorphins in Alzheimer's disease and age-related cognitive deficits, Neurodegener. Dis. [Internet] 13 (2014) 82–85. Available from: https://www.karger.com/Article/FullText/353848.

[2] T. Yakovleva, Z. Marinova, A. Kuzmin, N.G. Seidah, V. Haroutunian, L. Terenius, et al., Dysregulation of dynorphins in Alzheimer disease, Neurobiol. Aging [Internet] 28 (2007) 1700–1708. Available from: http://www.ncbi.nlm.nih.gov/pubmed/16914231.

[3] G.Y. Bakalkin, A.B. Rakhmaninova, V.K. Akparov, A.A. Volodin, V.V. Ovchinnikov, R.A. Sarkisyan, Amino acid sequence pattern in the regulatory peptides, Int. J. Pept. Protein Res. [Internet] 38 (1991) 505–510. Available from: http://www.ncbi.nlm.nih.gov/pubmed/1668097.

[4] W. Fischli, A. Goldstein, M.W. Hunkapiller, L.E. Hood, Two "big" dynorphins from porcine pituitary, Life Sci. 31 (1982) 1769–1772.

[5] W. Fischli, A. Goldstein, M.W. Hunkapillert, L.E. Hoodt, Isolation and amino acid sequence analysis of a 4,000-dalton dynorphin from porcine pituitary (opioid/peptide/endorphin/neuropeptide/prohormone) [Internet], Proc. Natl. Acad. Sci. U. S. A. 79 (1982) 5435–5437. Available from: https://www.pnas.org.

[6] Z. Marinova, V. Vukojević, S. Surcheva, T. Yakovleva, G. Cebers, N. Pasikova, et al., Translocation of dynorphin neuropeptides across the plasma membrane, J. Biol. Chem. [Internet] 280 (2005) 26360–26370. Available from: https://linkinghub.elsevier.com/retrieve/pii/S0021925820568294.

[7] L. Hugonin, V. Vukojević, G. Bakalkin, A. Gräslund, Calcium influx into phospholipid vesicles caused by dynorphin neuropeptides, Biochim. Biophys. Acta Biomembr. [Internet] 1778 (2008) 1267–1273. Available from: https://www.sciencedirect.com/science/article/pii/S000527360800076X.

[8] L. Hugonin, V. Vukojević, G. Bakalkin, A. Gräslund, Membrane leakage induced by dynorphins, FEBS Lett. [Internet] 580 (2006) 3201–3205. Available from: https://www.sciencedirect.com/science/article/pii/S0014579306005357.

[9] K.F. Hauser, J.K. Foldes, C.S. Turbek, Dynorphin a (1−13) neurotoxicity in vitro: opioid and non-opioid mechanisms in mouse spinal cord neurons, Exp. Neurol. [Internet] 160 (1999) 361–375. Available from: https://www.ncbi.nlm.nih.gov/pmc/articles/PMC4868554/.

[10] L.M. Alvero-Gonzalez, D.A. Perini, M. Queralt-Martín, A. Perálvarez-Marín, C. Viñas, A. Alcaraz, Probing electrophysiological activity of amphiphilic dynorphin A in planar neutral membranes reveals both ion channel-like activity and neuropeptide translocation, Bioelectrochem. (Amsterdam, Neth.). 154 (2023) 108527, https://doi.org/10.1016/j.bioelechem.2023.108527.

[11] O. Maximyuk, V. Khmyz, C.-J. Lindskog, V. Vukojević, T. Ivanova, I. Bazov, et al., Plasma membrane poration by opioid neuropeptides: a possible mechanism of pathological signal transduction, Cell Death Dis. [Internet] 6 (2015) e1683–e1683. Available from: https://www.nature.com/articles/cddis201539.

[12] L. Gallego-Villarejo, C. Wallin, S. Król, J. Enrich-Bengoa, A. Suades, M. Aguilella-Arzo, et al., Big dynorphin is a neuroprotector scaffold against amyloid β-peptide aggregation and cell toxicity, Comput. Struct. Biotechnol. J. [Internet] 20 (2022) 5672–5679. Available from: https://linkinghub.elsevier.com/retrieve/pii/S2001037022004615.

[13] Y. Kanemitsu, M. Hosoi, P.J. Zhu, F.F. Weight, R.W. Peoples, J.S. McLaughlin, L. Zhang, Dynorphin a inhibits NMDA receptors through a pH-dependent mechanism, Mol. Cell. Neurosci. 24 (3) (2003) 525–537, https://doi.org/10.1016/s1044-7431(03)00214-8.

[14] G. Bakalkin, H. Watanabe, J. Jezierska, C. Depoorter, C. Verschuuren-Bemelmans, I. Bazov, et al., Prodynorphin mutations cause the neurodegenerative disorder spinocerebellar ataxia type 23, Am. J. Hum. Genet. [Internet] 87 (2010) 593–603. Available from: https://linkinghub.elsevier.com/retrieve/pii/S0002929710005161.

[15] F. Madani, M.M. Taqi, S.K.T.S. Wärmländer, D.S. Verbeek, G. Bakalkin, A. Gräslund, Perturbations of model membranes induced by pathogenic dynorphin a mutants causing neurodegeneration in human brain, Biochem. Biophys. Res. Commun. [Internet] 411 (2011) 111–114. Available from: https://linkinghub.elsevier.com/retrieve/pii/S0006291X11010850.
[16] J. Björnerås, A. Gräslund, L. Mäler, Membrane interaction of disease-related Dynorphin A variants, Biochem. Int. 52 (2013) 4157–4167. Available from: https://pubs.acs.org/doi/10.1021/bi4004205.
[17] C.J.L.M. Smeets, J. Zmorzyńska, M.N. Melo, A. Stargardt, C. Dooley, G. Bakalkin, et al., Altered secondary structure of Dynorphin A associates with loss of opioid signalling and NMDA-mediated excitotoxicity in SCA23, Hum. Mol. Genet. 25 (2016) 2728–2737. Available from: https://academic.oup.com/hmg/article-lookup/doi/10.1093/hmg/ddw130.
[18] R. Sankararamakrishnan, H. Weinstein, Molecular dynamics simulations predict a tilted orientation for the helical region of Dynorphin A (1–17) in dimyristoylphosphatidylcholine bilayers, Biophys. J. [Internet] 79 (2000) 2331–2344. Available from: https://linkinghub.elsevier.com/retrieve/pii/S0006349500764794.
[19] R. Sankararamakrishnan, H. Weinstein, Positioning and stabilization of dynorphin peptides in membrane bilayers: the mechanistic role of aromatic and basic residues revealed from comparative MD simulations [cited 2023 Jul 27]; Available from: https://pubs.acs.org/sharingguidelines, 2002.
[20] A. Kira, N. Javkhlantugs, T. Miyamori, Y. Sasaki, M. Eguchi, I. Kawamura, et al., Interaction of extracellular loop II of κ-opioid receptor (196–228) with opioid peptide dynorphin in membrane environments as revealed by solid state nuclear magnetic resonance, quartz crystal microbalance and molecular dynamics simulation, J. Phys. Chem. B [Internet] 118 (2014) 9604–9612. Available from: https://pubs.acs.org/doi/abs/10.1021/jp505412j [cited 2024 Dec 19].
[21] D.A. Perini, M. Aguilella-Arzo, A. Alcaraz, A. Perálvarez-Marín, M. Queralt-Martín, Dynorphin a induces membrane permeabilization by formation of proteolipidic pores. Insights from electrophysiology and computational simulations, Comput. Struct. Biotechnol. J. [Internet] 20 (2022) 230–240. Available from: https://linkinghub.elsevier.com/retrieve/pii/S2001037021005304.
[22] C. Kutzner, H. Grubmüller, B.L. De Groot, U. Zachariae, Computational electrophysiology: the molecular dynamics of ion channel permeation and selectivity in atomistic detail, Biophys. J. [Internet] 101 (2011) 809 ([cited 2023 Jul 4]. Available from: /pmc/articles/PMC3175076/).
[23] S. Yesylevskyy, S.J. Marrink, A.E. Mark, Alternative mechanisms for the interaction of the cell-penetrating peptides penetratin and the TAT peptide with lipid bilayers, Biophys. J. 97 (2009) 40–49.
[24] D.M. Copolovici, K. Langel, E. Eriste, Ü. Langel, Cell-penetrating peptides: design, synthesis, and applications, ACS Nano [Internet] 8 (2014) 1972–1994. Available from: https://pubs.acs.org/doi/10.1021/nn4057269.
[25] F. Milletti, Cell-penetrating peptides: classes, origin, and current landscape, Drug Discov. Today [Internet] 17 (2012) 850–860. Available from: http://www.ncbi.nlm.nih.gov/pubmed/22465171.
[26] L. Hugonin, A. Barth, A. Gräslund, A. Perálvarez-Marín, Secondary structure transitions and aggregation induced in dynorphin neuropeptides by the detergent sodium dodecyl sulfate, Biochim. Biophys. Acta Biomembr. [Internet] 1778 (2008) 2580–2587. Available from: https://www.sciencedirect.com/science/article/pii/S0005273608002198.
[27] G.M. Torrie, J.P. Valleau, Nonphysical sampling distributions in Monte Carlo free-energy estimation: umbrella sampling, J. Comput. Phys. 23 (1977) 187–199.
[28] K. Huang, A.E. García, Free energy of translocating an arginine-rich cell-penetrating peptide across a lipid bilayer suggests pore formation, Biophys. J. 104 (2013) 412–420.
[29] Y. Hu, X. Liu, S.K. Sinha, S. Patel, Translocation thermodynamics of linear and cyclic nonaarginine into model dppc bilayer via coarse-grained molecular dynamics simulation: implications of pore formation and nonadditivity, J. Phys. Chem. B 118 (2014) 2670–2682.
[30] W.G. Noid, J.W. Chu, G.S. Ayton, V. Krishna, S. Izvekov, G.A. Voth, et al., The multiscale coarse-graining method. I. a rigorous bridge between atomistic and coarse-grained models, J. Chem. Phys. [Internet] 128 (2008) [cited 2024 Dec 19]. Available from: https://pubmed.ncbi.nlm.nih.gov/18601324/.
[31] J. Gimenez-Dejoz, K. Numata, Molecular dynamics study of the internalization of cell-penetrating peptides containing unnatural amino acids across membranes, Nanoscale Adv. 4 (2022) 397–407.
[32] E. Catalina-Hernandez, M. Aguilella-Arzo, A. Peralvarez-Marin, M. Lopez-Martin, Computational insights into membrane disruption by cell-penetrating peptides, J. Chem. Inf. Model. [Internet] 65 (2025) 1549–1559. Available from: https://pubs.acs.org/doi/full/10.1021/acs.jcim.4c01940 [cited 2025 Jan 22].
[33] D.A. Case, K. Belfon, I.Y. Ben-Shalom, S.R. Brozell, D.S. Cerutti, T.E. Cheatham, et al., AMBER 2020, 2020.
[34] J.A. Maier, C. Martinez, K. Kasavajhala, L. Wickstrom, K.E. Hauser, C. Simmerling, Ff14SB: improving the accuracy of protein side chain and backbone parameters from ff99SB, J. Chem. Theory Comput. 11 (2015) 3696–3713, https://doi.org/10.1021/acs.jctc.5b00255.
[35] V. Kräutler, W.F. van Gunsteren, P.H. Hünenberger, A fast SHAKE algorithm to solve distance constraint equations for small molecules in molecular dynamics simulations, J. Comput. Chem. [Internet] 22 (2001) 501–508. Available from: https://onlinelibrary.wiley.com/doi/abs/10.1002/1096-987X%2820010415%2922%3A5%3C501%3A%3AAID-JCC1021%3E3.0.CO%3B2-V.
[36] B.R. Brooks, C.L. Brooks III, A.D. Mackerell Jr., L. Nilsson, R.J. Petrella, B. Roux, et al., CHARMM: the biomolecular simulation program, J. Comput. Chem. [Internet] 30 (2009) 1545–1614. Available from: https://onlinelibrary.wiley.com/doi/abs/10.1002/jcc.21287.
[37] J. Lee, X. Cheng, J.M. Swails, M.S. Yeom, P.K. Eastman, J.A. Lemkul, S. Wei, J. Buckner, J.C. Jeong, Y. Qi, S. Jo, V.S. Pande, D.A. Case, C.L. Brooks, A. D. MacKerell, J.B. Klauda, W. Im, CHARMM-GUI input generator for NAMD, GROMACS, AMBER, OpenMM, and CHARMM/OpenMM simulations using the CHARMM36 additive force field, J. Chem. Theory Comput. 12 (1) (2016) 405–413, https://doi.org/10.1021/acs.jctc.5b00935.
[38] S. Jo, T. Kim, V.G. Iyer, W. Im, CHARMM-GUI: a web-based graphical user interface for CHARMM, J. Comput. Chem. [Internet] 29 (2008) 1859–1865. Available from: https://onlinelibrary.wiley.com/doi/abs/10.1002/jcc.20945.
[39] J. Lee, D.S. Patel, J. Ståhle, S.-J. Park, N.R. Kern, S. Kim, X. Cheng, M.A. Valvano, O. Holst, Y.A. Knirel, Y. Qi, S. Jo, J.B. Klauda, G. Widmalm, W. Im, CHARMM-GUI membrane builder for complex biological membrane simulations with glycolipids and lipoglycans, J. Chem. Theory Comput. [Internet] 15 (1) (2019) 775–786, https://doi.org/10.1021/acs.jctc.8b01066.
[40] S. Jo, J.B. Lim, J.B. Klauda, W. Im, CHARMM-GUI membrane builder for mixed bilayers and its application to yeast membranes, Biophys. J. 97 (2009) 50–58.
[41] J. Lee, M. Hitzenberger, M. Rieger, N.R. Kern, M. Zacharias, W. Im, CHARMM-GUI supports the amber force fields, J. Chem. Phys. 153 (2020) 35103.
[42] E.L. Wu, X. Cheng, S. Jo, H. Rui, K.C. Song, E.M. Dávila-Contreras, et al., CHARMM-GUI membrane builder toward realistic biological membrane simulations, J. Comput. Chem. 35 (2014) 1997–2004. Available from: https://onlinelibrary.wiley.com/doi/abs/10.1002/jcc.23702.
[43] C.J. Dickson, R.C. Walker, I.R. Gould, Lipid21: complex lipid membrane simulations with AMBER, J. Chem. Theory Comput. 18 (2022) 1726–1736, https://doi.org/10.1021/acs.jctc.1c01217.
[44] R.X. Gu, S. Baoukina, Peter D. Tieleman, Phase separation in atomistic simulations of model membranes, J. Am. Chem. Soc. [Internet] 142 (2020) 2844–2856. Available from: https://pubs.acs.org/doi/epdf/10.1021/jacs.9b11057 [cited 2025 Jan 29].
[45] G. Hummer, A. Szabo, Free energy reconstruction from nonequilibrium single-molecule pulling experiments, Proc. Natl. Acad. Sci. [Internet] 98 (2001) 3658–3661. Available from: https://www.pnas.org/doi/10.1073/pnas.071034098.
[46] C. Jarzynski, Nonequilibrium equality for free energy differences, Phys. Rev. Lett. [Internet] 78 (1997) 2690–2693. Available from: https://link.aps.org/doi/10.1103/PhysRevLett.78.2690.
[47] S. Park, K. Schulten, Calculating potentials of mean force from steered molecular dynamics simulations [cited 2023 Jul 11]; Available from: http://jcp.aip.org/jcp/copyright.jsp, 2004.
[48] N. Michaud-Agrawal, E.J. Denning, T.B. Woolf, O. Beckstein, MDAnalysis: a toolkit for the analysis of molecular dynamics simulations, J. Comput. Chem. [Internet] 32 (2011) 2319–2327 [cited 2023 Jul 24]. Available from: https://pubmed.ncbi.nlm.nih.gov/21500218/.
[49] R. Gowers, M. Linke, J. Barnoud, T. Reddy, M. Melo, S. Seyler, et al., MDAnalysis: a Python package for the rapid analysis of molecular dynamics simulations, in: Python in Science Conference [Internet], 2016, pp. 98–105. Available from: https://conference.scipy.org/proceedings/scipy2016/oliver_beckstein.html.
[50] W. Song, R.A. Corey, T.B. Ansell, C.K. Cassidy, M.R. Horrell, A.L. Duncan, et al., PyLipID: a python package for analysis of protein–lipid interactions from molecular dynamics simulations, J. Chem. Theory Comput. [Internet] 18 (2022) 1188–1201. Available from: https://pubs.acs.org/doi/10.1021/acs.jctc.1c00708.
[51] J.D. Hunter, Matplotlib: a 2D graphics environment, Comput. Sci. Eng. 9 (2007) 90–95.
[52] M.L. Waskom, Seaborn: statistical data visualization, J. Open Source Softw. [Internet] 6 (2021) 3021 [cited 2023 Sep 24]. Available from: https://joss.theoj.org/papers/10.21105/joss.03021.
[53] E.F. Pettersen, T.D. Goddard, C.C. Huang, E.C. Meng, G.S. Couch, T.I. Croll, et al., UCSF chimeraX: structure visualization for researchers, educators, and developers, Protein Sci. [Internet] 30 (2021) 70–82. Available from: https://onlinelibrary.wiley.com/doi/pdfdirect/10.1002/pro.3943.
[54] T.D. Goddard, C.C. Huang, E.C. Meng, E.F. Pettersen, G.S. Couch, J.H. Morris, et al., UCSF chimerax: meeting modern challenges in visualization and analysis, Protein Sci. [Internet] 27 (2018) 14–25. Available from: https://europepmc.org/articles/pmc5734306?pdf=render.
[55] W. Humphrey, A. Dalke, K. Schulten, VMD: visual molecular dynamics, J. Mol. Graph. [Internet] 14 (1996) 33–38 [cited 2023 Jul 24]. Available from: https://pubmed.ncbi.nlm.nih.gov/8744570/.
[56] R. Elber, Defect formation and peptide permeation across phospholipid membranes, J. Phys. Chem. B 127 (2023) 7810–7818 [cited 2023 Sep 20]; Available from: https://pubs.acs.org/doi/10.1021/acs.jpcb.3c04895.
[57] F. Her Choong, Yap B. Keat, Cell-penetrating peptides: correlation between peptide-lipid interaction and penetration efficiency, ChemPhysChem 22 (2021) 493–498.
[58] J.L. MacCallum, W.F.D. Bennett, D.P. Tieleman, Transfer of arginine into lipid bilayers is nonadditive, Biophys. J. 101 (2011) 110–117.
[59] S. Choe, Translocation of a single Arg9 peptide across a DOPC/DOPG(4:1) model membrane using the weighted ensemble method, Sci. Rep. 13 (2023) 1–9 [cited 2023 Sep 24]. Available from: https://www.nature.com/articles/s41598-023-28493-4.
[60] W.F.D. Bennett, C.K. Hong, Y. Wang, D.P. Tieleman, Antimicrobial peptide simulations and the influence of force field on the free energy for pore formation in lipid bilayers, J. Chem. Theory Comput. [Internet] 12 (2016) 4524–4533 [cited 2025 Feb 26]. Available from: https://pubs.acs.org/doi/full/10.1021/acs.jctc.6b00265.

[61] D. Sengupta, H. Leontiadou, A.E. Mark, S.J. Marrink, Toroidal pores formed by antimicrobial peptides show significant disorder, Biochim. Biophys. Acta Biomembr. 1778 (2008) 2308–2317.
[62] J.D. Richardson, R.C. Van Lehn, Free energy analysis of peptide-induced pore formation in lipid membranes by bridging atomistic and coarse-grained simulations, J. Phys. Chem. B 128 (2024) 8737–8752, https://doi.org/10.1021/acs.jpcb.4c03276.
[63] Z.A. Levine, P.T. Vernier, Life cycle of an electropore: field-dependent and field-independent steps in pore creation and annihilation, J. Membr. Biol. 236 (2010) 27–36.
[64] J. Repáková, J.M. Holopainen, M.R. Morrow, M.C. McDonald, P. Čapková, I. Vattulainen, Influence of DPH on the structure and dynamics of a DPPC bilayer, Biophys. J. 88 (2005) 3398–3410.
[65] S.L. Regen, Cholesterol's condensing effect: unpacking a century-old mystery, JACS Au 2 (2022) 84–91, https://doi.org/10.1021/jacsau.1c00493.
[66] M. Jain, S. Matysiak, Dual role of anionic lipids in amyloid aggregation, J. Phys. Chem. B 128 (44) (2024) 10831–10840, https://doi.org/10.1021/acs.jpcb.4c05636.
[67] F. Zakany, I.M. Mándity, Z. Varga, G. Panyi, P. Nagy, T. Kovacs, Effect of the lipid landscape on the efficacy of cell-penetrating peptides, Cells 12 (2023) 1700 [cited 2024 Feb 16]. Available from: https://www.mdpi.com/2073-4409/12/13/1700/htm.
[68] J. Pae, P. Säälik, L. Liivamägi, D. Lubenets, P. Arukuusk, Ü. Langel, et al., Translocation of cell-penetrating peptides across the plasma membrane is controlled by cholesterol and microenvironment created by membranous proteins, J. Control. Release 192 (2014) 103–113.
[69] J. Lind, A. Gräslund, L. Mäler, Membrane interactions of Dynorphins, Biochem. Int. 45 (2006) 15931–15940. Available from: https://pubs.acs.org/doi/10.1021/bi061199g.
[70] H.D. Herce, A.E. Garcia, Molecular dynamics simulations suggest a mechanism for translocation of the HIV-1 TAT peptide across lipid membranes, Proc. Natl. Acad. Sci. U. S. A. [Internet] 104 (2007) 20805–20810. Available from: https://www.pnas.org/doi/full/10.1073/pnas.0706574105.
[71] E. Trofimenko, G. Grasso, M. Heulot, N. Chevalier, M.A. Deriu, G. Dubuis, et al., Genetic, cellular, and structural characterization of the membrane potential-dependent cell-penetrating peptide translocation pore, Elife [Internet] 10 (2021) ([cited 2023 Jul 13]. Available from: /pmc/articles/PMC8639150/).
[72] P. Stothard, The sequence manipulation suite: JavaScript programs for analyzing and formatting protein and DNA sequences, BioTechniques 28 (2000) 1102–1104, https://doi.org/10.2144/00286ir01.